INVITED PAPER

Adaptive Transmission With Single-Carrier Multilevel BICM

Higher total throughput can be achieved with Bit Interleaved Coded Modulation (BICM) by using a different code-selection for each of the multiple modulation components made possible by this technique.

By Tad Matsumoto, *Senior Member IEEE*, Shinsuke Ibi, *Member IEEE*, Seiichi Sampei, *Fellow IEEE*, and Reiner Thomä, *Fellow IEEE*

ABSTRACT | In this paper, we introduce adaptive link control techniques for multiple-input multiple-output (MIMO) systems with broadband single-carrier signaling. Soft cancellation and minimum mean squared error turbo equalization is assumed, where matching between coding and equalization plays crucial roles to achieve high throughput. This paper uses multilevel coded bit-interleaved coded modulation (ML-BICM) with linear mapping as a core part of the transmission, on top of which this paper applies automatic repeat request (ARQ) with adaptive coding (AC) for link control. The reason behind the use of the linear mapping ML-BICM is the separability between the layers in the modulation format: This should bring us a significant benefit in designing the link control strategies because each layer has its own reliability, and the adaptive link control should be optimized based on the each layer's reliabilities. For ARQ with ML-BICM, we introduce layer-by-layer retransmission control, where turbo equalization and retransmission control can be performed independently over the layers because of the layer-separability. The layer-by-layer concept is then applied to AC with ML-BICM, where the code parameters such as code rate and generator polynomials are chosen so that after several iterations the mutual information between the transmitted and the soft-input soft-output decoder output information can reach a value very close to *one* while minimizing the rate loss due to the mismatch between the equalization and decoder. Extrinsic information transfer analysis is performed for the MIMO channel realization being given. The transmitter is notified of the selected codes for the each layer via the feedback channel, and uses the selected codes for the following transmission, assuming that the channel state information (CSI) stays the same at least over two consecutive frames. Finally, this paper evaluates the throughput performances of the ML-BICM ARQ and AC techniques using multidimensional field measurement data. The performance tendencies are correlated with propagation properties, obtained as results of the high-resolution channel analysis, such as spatial spreads at the transmitter and receiver sides.

KEYWORDS | Adaptive rate control; bit-interleaved coded modulation (BICM); channel sounding; extrinsic information transfer (EXIT) chart; turbo equalization

I. INTRODUCTION

Equalization of severe frequency-selective channels has long been one of the core topics for the research community seeking for the opportunity of single carrier's revival in broadband mobile communications. The technologies used by our legacy commercial systems are mainly aiming at the *mitigation* of the undesirable effects of intersymbol interference (ISI) caused by the channel's severe frequency selectivity. In code-division multiple-access (CDMA) systems, such ISI mitigation is achieved through the *despreading* process at the receiver, where the multipath components are first *decomposed* into the separated multiple correlation peaks that can then be combined to achieve path diversity improvement. However, since all simultaneous users share the same frequency band, the most crucial issue with CDMA systems is the resistance against multiple-access interference.

Manuscript received December 15, 2006; revised May 2, 2007.
T. Matsumoto is with Japan Advanced Institute of Science and Technology, Ishikawa 923-1292, Japan. He is also with the Centre for Wireless Communications, University of Oulu, 90570 Oulu, Finland (e-mail: matumoto@jaist.ac.jp; tadashi.matsumoto@ee.oulu.fi).
S. Ibi and **S. Sampei** are with Department of Information and Communications Technology, Graduate School of Engineering, Osaka University, Osaka 565-0871, Japan (e-mail: ibi@comm.eng.osaka-u.ac.jp; sampei@comm.eng.osaka-u.ac.jp).
R. Thomä is with the Electronic Measurement Research Laboratory, Ilmenau University of Technology, D-98684 Ilmenau, Germany (e-mail: Reiner.Thomae@TU-Ilmenau.de).
Digital Object Identifier: 10.1109/JPROC.2007.904441

In orthogonal frequency-division-multiplexing (OFDM) systems, the ISI mitigation is a built-in capability of the transmitted signal waveform, where the subcarriers are ISI-free because the bandwidth of the subcarriers is small enough compared to the channel coherence bandwidth: The circulant structure of the channel, resulting from adding at the head of each OFDM block the cyclic prefix (CP) larger than the channel delay spread, allows the receiver to demodulate the received signal by performing the discrete Fourier transform (DFT). However, a negative effect due to summing up the multiple orthogonal subcarriers to construct one OFDM symbol is the increased peak-to-average power ratio, which requires a relatively wide range of amplifier linearity for the OFDM signal transmission.

Single-carrier signal transmission does not require such a wide range amplifier linearity as in OFDM, and is suitable especially for uplink where the life longevity of handset batteries is a crucial requirement. However, the channel memory length, over which ISI, due to a single symbol, lasts, is very large in broadband single-carrier signal transmission. For example, if a signal with the symbol rate of 100 Msymbol/s is transmitted over a channel having 0.5-μs delay spread, the channel memory length reaches 50 symbols. Therefore, the fact that the computational complexity for the optimal ISI equalization increases exponentially with the channel memory length L, counted in symbols, has long been believed to be a bottleneck hostility of the problem.

The single-carrier wireless communication research community has experienced two crucial discoveries in the last 15 years, turbo coding and frequency-domain (FD) equalization techniques. The turbo principle is an extension of the turbo decoding technique to more generic "decision-making" process: Knowing that the channel can be modeled as a tapped delay line, the multipath propagation can be seen as a process of taking convolution between the transmitted symbol sequence and the channel, which, in turn, can be interpreted in an information theoretic terminology as being equivalent to convolutional coding, defined in the *complex* domain. Then, the coded transmission system can be seen as a serially concatenated system, of which the outer code is the channel code used and the inner code is the multipath channel. Now, given the interpretation above, we know that we can use the turbo "decoding" techniques when "detecting" the signal suffering from ISI. This concept is referred to as "turbo equalization."

In turbo equalization, soft-information that expresses the ratio of the probability of a bit being one versus being zero, referred to as likelihood ratio, is exchanged between the equalizer part and the decoder part. To produce the soft-output information, both the equalizer and decoder have to perform the "maximum *a posteriori* probability (MAP)" algorithm, e.g., [1]. Several reduced complexity versions of MAP are also known, however, they all use the trellis diagram of the "code." As noted above, the multipath channel can be viewed as a complex-valued convolutional code, and therefore, if the channel has a large memory length, the computational complexity for the MAP equalization increases exponentially, and becomes still prohibitively high: This invokes the necessity to replace the MAP equalization part with a reduced-complexity soft-input soft-output (SISO) equalizer.

Suboptimal versions of turbo equalization have been known to achieve excellent performances without requiring as heavy a computational effort as the MAP equalizer. Among them, this paper concentrates on the particular turbo equalization algorithm presented in [2]–[4] for broadband single-carrier signaling. The original turbo-equalization algorithms of [2]–[4] consist of soft interference cancellation using symbol estimates computed from the channel decoder feedback, followed by (time-domain) linear time-variant MMSE filtering and soft symbol demapping. It has been shown [5] that the algorithm of [2]–[4] can be extended to multiple-input multiple-output (MIMO) systems. With the soft interference cancellation and MMSE equalization, the heaviest part of computation is the inversion of the covariance matrix for the interference residual, which, however, may still be intractable, if the channel memory length and/or the number N of the received antennas become large: The required complexity for the time-domain covariance matrix inversion is at a cubic order of $L \times N$.

The other crucial event experienced recently by the single-carrier wireless communication research community is the reformulation of frequency domain equalization techniques [6], [7], where by using the CP-transmission for single-carrier signaling, the received signal is converted into the frequency domain, and the signal processing performed frame-by-frame. With the FD processing, the computational complexity can be reduced significantly to a logarithmic order of the frame length. The frequency domain reformulation of linear equalization as well as decision feedback equalization based on minimum mean squared error (MMSE) criterion has been derived and their performances presented in [6]. Furthermore, it is shown [8] that the frequency domain technique can be extended to an MIMO system. In fact, the matrix inversion is still involved in frequency domain algorithms, but the size of the matrix that has to be inverted is $N \times N$, which no longer depends on the channel memory length. Obviously, the complexity for this is much less than the time-domain MIMO equalization algorithms.

Now, given the two crucial technological bases made available, efforts henceforth should be directed to combining the two ideas, and to taking more benefits from them. References [9]–[11] derive FD turbo equalization algorithms based on the soft interference cancellation and MMSE filtering technique, and [11] derives frequency domain decision feedback turbo equalization algorithm. The frequency domain turbo equalization can, in common,

achieve excellent performance without requiring excessive computational efforts.

Adaptive transmission is very suitable for OFDM signaling because one *single* OFDM symbol bears modulations on each subcarrier, and it can choose the modulation multiplicity considered most preferable (known as the bit-loading merit), if the transmitter has the knowledge of each subcarrier's received signal-to-noise power ratio (SNR). Furthermore, each subcarrier's transmit power is determined so that the sum-capacity is maximized, according to the water-filling criterion, while the total transmit power is kept constant. Single-carrier signaling has long been believed to be unsuitable for adaptive transmission because the whole bandwidth is occupied by a single sequence, for which the transmission chain can not take the bit-loading merit.

However, since the usefulness of the maximum MAP algorithm applied to symbol-to-bit likelihood demapping in bit-interleaved coded modulation (BICM) [12], another dimensionality in attaining the design flexibility has arisen for the single-carrier adaptive transmission: If the system uses linear mapping by which the constellation is constructed through the super-positioning of smaller modulation *components*, which are referred to as "layers" in this paper, the demapper can "decompose" the whole constellation into the layers: The system uses multiple encoders and SISO decoders, and equalization-decoding chain performs the log likelihood ratio (LLR) exchange independently of other layers. This structure, referred to as multilevel (ML)-BICM, makes coding and modulation as well as packet-wise retransmission control *independent* among the layers.

Now, the unequal error protection (UEP) provided with ML-BICM [13], [14] can be exploited to offer another dimensionality in wireless link adaptation. If the code parameters such as rate and generator polynomials can be determined so that the selected code is well matched to the turbo equalizer's convergence properties at each layer, the total throughput should be significantly improved. This leads to a concept of *layer-by-layer* adaptive coding (AC), based on extrinsic information transfer (EXIT) analysis, where the instantaneous channel state information (CSI) is assumed to stay the same over, at least, two consecutive frames, and based on the result of the EXIT analysis for the firtst frame, the receiver selects the code parameters from among the code set available. The selected code parameters for the layers are then sent back to the transmitter via the feedback channel, and used for the transmission of the second frame.

Layer-by-layer automatic repeat request (L-ARQ) with AC can effectively exploit the UEP supported by ML-BICM. By performing ARQ protocols independently over the layers, different throughput efficiencies among the layers can be achieved, which in turn can be viewed as *layer-by-layer* link adaptation through retransmission. This technique, referred to as ML-BICM with AC, can achieve much higher total throughput over single ARQ (S-ARQ) with BICM or ML-BICM, where the bit-wise LLR calculated from the equalizer output symbols are all mixed in one frame and used for SISO decoding of the channel code.[1]

The primary goal of this paper is to exploit the design flexibility supported by ML-BICM turbo equalization for adaptive single-carrier transmission over broadband mobile communication channels. This paper is organized as follows. The system model used in this paper is presented in Section II, where the algorithm for the frequency domain soft cancellation and MMSE (SC-MMSE) filtering BICM equalization, according to [9] and [10], is briefly explained. EXIT properties of ML-BICM are introduced in Section III, and a *layer-by-layer* code selection technique based on EXIT analysis for ML-BICM, which is one of the most significant contributions of this paper, is presented in Section IV. L-ARQ with ML-BICM as well as L-ARQ with ML-BICM AC is presented and their performance compared with S-ARQ with BICM in Section IV. Section V briefly describes outage-based code optimization techniques, where *only* average CSI is assumed to be available. Sections III, IV, and V assume FD SC-MMSE. Section VI presents measurement data-based performance evaluation results for the adaptive code selection and ARQ techniques, where measurement data collected at a courtyard of Ilmenau University of Technology, Germany, is used. The paper is concluded with a summary.

II. SYSTEM MODEL

A. Channel

The system that this paper assumes employs M Tx and N Rx antennas, where symbols to be transmitted are spatially multiplexed and sent from the multiple Tx antennas. Let the complex baseband signal to be transmitted from the mth Tx antenna at the *discrete* kth symbol timing be denoted by $s_m(k)$. Also, let the channel impulse response (CIR) between the mth Tx and the nth Rx antennas, superimposed with the Tx and Rx filters, be denoted by $h_{n,m}(t = lT_s) = h_{n,m}(l)$ with T_s being the symbol duration. The discrete-time representation $r_n(k)$ of the received symbol received by the nth Rx antenna is given by

$$r_n(k) = \sum_{l=0}^{L-1} \sum_{m=1}^{M} h_{n,m}(l) s_m(k-l) + \nu_n(k) \qquad (1)$$

where L denotes the channel memory length, and $\nu_n(k)$ zero mean additive white Gaussian noise sample with variance N_0.

[1]Adaptive trellis coded BICM with S-ARQ may also attain the similar throughput gain over without AC. To the authors' knowledge, however, such a technique is not known, and therefore, it is out of the scope of this paper.

To allow for the frequency domain processing to be performed at the receiver side, a length P-symbol CP is appended to the head of the block comprised of K coded symbols, yielding each frame comprised of $P+K$ symbols. With the CP transmission, it is well known that after space- and time-sampling, the equivalent channel can be expressed by a block-circulant matrix, as summarized below: Removing CP at the receiver results in a vector notation of the channel as

$$\boldsymbol{r} = \boldsymbol{H}\boldsymbol{s} + \boldsymbol{\nu} \tag{2}$$

where $\boldsymbol{r}$, $\boldsymbol{s}$, and $\boldsymbol{\nu}$ are the received signal, the transmitted signal, and the Gaussian noise vectors, respectively, given by

$$\boldsymbol{r} = \left[\boldsymbol{r}_1^T, \cdots, \boldsymbol{r}_n^T, \cdots, \boldsymbol{r}_N^T\right]^T \tag{3}$$

$$\boldsymbol{s} = \left[\boldsymbol{s}_1^T, \cdots, \boldsymbol{s}_m^T, \cdots, \boldsymbol{s}_M^T\right]^T \tag{4}$$

and

$$\boldsymbol{\nu} = \left[\boldsymbol{\nu}_1^T, \cdots, \boldsymbol{\nu}_n^T, \cdots, \boldsymbol{\nu}_N^T\right]^T \tag{5}$$

with their component vectors being

$$\boldsymbol{r_n} = [r_n(1), \cdots, r_n(k), \cdots, r_n(K)]^T \tag{6}$$

$$\boldsymbol{s_m} = [s_m(1), \cdots, s_m(k), \cdots, s_m(K)]^T \tag{7}$$

and

$$\boldsymbol{\nu_n} = [\nu_n(1), \cdots, \nu_n(k), \cdots, \nu_n(K)]^T. \tag{8}$$

With the definitions of the terms above, the block circulant channel matrix can then be defined as

$$\boldsymbol{H} = [\boldsymbol{H}_1, \cdots, \boldsymbol{H}_m, \cdots, \boldsymbol{H}_M] \tag{9}$$

with its component submatrices being

$$\boldsymbol{H}_m = \left[\boldsymbol{H}_{1,m}^T, \cdots, \boldsymbol{H}_{n,m}^T, \cdots, \boldsymbol{H}_{N,m}^T\right] \tag{10}$$

and $\mathbf{H}_{n,m} = \mathrm{Circ}[h_{n,m}(0), \cdots, h_{n,m}(L-1), \mathbf{0}_{K-L}]^T$ comprised of its component vector being the argument of the Circ operator. $\mathbf{0}_x$ denotes an all-zeros vector with length x.

B. ML-BICM

A block diagram of the ML-BICM system assumed in this paper is shown in Fig. 1, where with M Tx antennas there are $MQ/2$ layers denoted as $\chi(m,q)$ $(m = 1, \cdots, M,$ and $q = 1, \cdots, Q/2)$ since the 2^Q quadrature amplitude modulation (QAM) signal consists of $Q/2$ layers. The quaternary phase-shift-keying (QPSK) signals of each layer are linearly weighted and summed up to construct a 2^Q QAM constellation. Note that the terminology "layer" corresponds to the QPSK sequence constituting the QAM constellation.

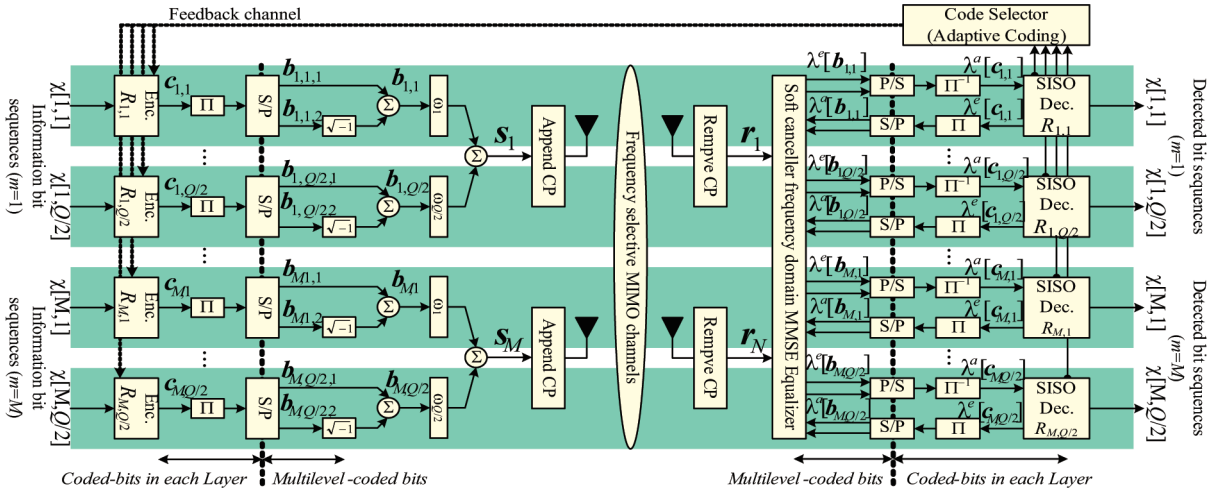

Fig. 1. *System block diagram.*

Now, in order to derive frequency domain MIMO SC-MMSE, we first define the following block-wise coded bit vector to be transmitted over the layer $\chi(m,q)$, as

$$\boldsymbol{c_{m,q}} = \left[c_{m,q}(1), \cdots, c_{m,q}(k'), \cdots, c_{m,q}(2K)\right]^T \tag{11}$$

where with $c_{m,q}(k') \in \{\pm 1\}$, k' denotes the bit index after encoding, and $2K$ the length of the encoded *bit* vector to be transmitted from the layer. Note that since each layer transmits the signal over the in-phase and quadrature channels, denoted as I- and Q-channels, respectively, for convenience, the length of the encoded bit vector is $2K$. Each layer's coded bit sequence $\boldsymbol{c}_{m,q}$ is then interleaved and serial-to-parallel (S/P) converted into two binary sequences, each having K bits to be transmitted over I- or Q-channels of the layer. Let us define the following block-wise QPSK *symbol* vector:

$$\begin{aligned}\boldsymbol{b_{m,q}} = \Big[&b_{m,q,1}(1) + \sqrt{-1}b_{m,q,2}(1), \cdots, b_{m,q,1}(k) \\ &+ \sqrt{-1}b_{m,q,2}(k), \cdots, b_{m,q,1}(K) \\ &+ \sqrt{-1}b_{m,q,2}(K)\Big]^T\end{aligned} \tag{12}$$

where k denotes the bit index after S/P conversion and $b_{m,q,j}(k) \in \{\pm 1\}$ is, with $j = 1$ and 2 corresponding to the I- and Q-channels, respectively. Linear mapping is used to construct the 2^Q QAM constellation for ML-BICM, with which the transmitted signal vector s_m is expressed as

$$\boldsymbol{s_m} = \sum_{q=1}^{Q/2} \omega_q \boldsymbol{b_{m,q}} \tag{13}$$

where the mapping coefficients are defined as

$$[\omega_1, \cdots, \omega_{Q/2}] = \begin{cases} [1] & /\sqrt{2} \quad (Q=2) \\ [2\ 1] & /\sqrt{10} \quad (Q=4) \\ [4\ 2\ 1] & /\sqrt{42} \quad (Q=6). \end{cases} \tag{14}$$

Without AC, the encoders used by the each level are fixed regardless of channel realizations, while with AC, they are selected from among the available code set by the receiver; without AC, only binary information, Ack and Nack, are transmitted via the feedback channel for retransmission control, whereas with AC the transmitter is notified of the code selected for each layer.

C. Iterative Equalization and Decoding

Since there are plenty of articles that describe how the SC-MMSE equalizers work, only an outline of FD MIMO SC-MMSE for ML-BICM is provided in this section, which are summarized as follows.

1) After the removal of the CP part at the receiver, the received space–time sampled data corresponding to the whole single frame of interest is converted into FD by using a block-wise DFT matrix where the each received signal sample block from its corresponding received antenna is multiplied by a DFT matrix.
2) The frequency domain representation of the soft replica of interfering components is produced using the equivalent time-domain block-wise channel matrix $\boldsymbol{H}$. The soft bit estimates are calculated from the decoder feedback.
3) The FD interference soft replica is subtracted from the FD received signal.
4) Remaining interfering components are further suppressed by an FD MMSE filter vector $\boldsymbol{\Omega}_m(k)$ satisfying the criterion

$$\boldsymbol{\Omega}_m(k) = \arg\min_{\boldsymbol{\Omega}_m} \mathbb{E}\left[\|\boldsymbol{\Omega}_m \tilde{\boldsymbol{r}} - s_m(k)\|^2\right] \tag{15}$$

where $\tilde{\boldsymbol{r}}$ is the output of the FD soft interference cancellation in frequency domain. The $\tilde{\boldsymbol{r}}$ contains only the residual components of the soft canceller output, but with an exception that the frequency domain contributions of the symbol to be detected to the all receive antennas remain. Note that $\boldsymbol{\Omega}_m$ includes mathematical manipulations for converting the filter output to the time domain. With a minor approximation on the residual interference energy, the necessity for the symbol timing-wise calculation of the MMSE filter weight vector can be eliminated, and the weight vector as well as block-wise output of the equalizer can be calculated. For more details, please see [9] and [10].

5) Assuming that the MMSE filter output follows a Gaussian distribution, the equalizer output can be rewritten as

$$z_m(k) = \mu_m s_m(k) + \psi_m(k) \tag{16}$$

where μ_m and $\psi_m(k)$ represent equivalent amplitude level and zero mean independent complex Gaussian noise with variance σ_m^2, respectively. The derivation of μ_m and σ_m^2 can be found in [9] and [10]. Using the Gaussian approximation of (16), it is found that the probability density function (pdf) of $z_m(k)$, conditioned upon each symbol constellation point, takes a form of Gaussian density, and the extrinsic LLR $\lambda^e[b_{m,q,j}(k)]$ of the layer $\chi(m,q)$'s coded bit can

be computed by using the MAP algorithm. It should be emphasized that as described more quantitatively using EXIT chart in Section III, the layers $\chi(m,q)$ having different reliabilities are now separated with each other by the MAP algorithm. More details can be found in [12] and [15].

6) The obtained bit-wise extrinsic LLR is then forwarded to the SISO decoders via each layer's deinterleaver.

D. Numerical Comparison

Fig. 2(a) and (b) shows the bit-error rate (BER) versus symbol energy-to-noise spectral density ratio E_s/N_0 performances of FD SC-MMSE for QPSK [$Q=2$ in (14)] after the first and the eighth iterations, where $M=1$, $N=2$, and two 24-path frequency-selective channel realizations were assumed. Other simulation parameters are summarized in the figure caption. Fig. 2(a) is an example of the channel where FD SC-MMSE achieves a good performance, and Fig. 2(b) another, extreme, example where FD SC-MMSE achieves a bad performance. It is found by comparing those figures that the performance gain achieved by the turbo iterations is not significant in Fig. 2(a)'s channel, but it is significant in Fig. 2(b)'s channel.

It is well known that the asymptotic performance of turbo equalization, corresponding to the case where the decoder feedback is assumed to be perfect, is the maximum ratio combining path diversity bound [10]. However, their BER curves exhibit different convergence and asymptotic properties, depending on their channel realizations. This observation invokes the necessity of seeking for a better code design for turbo equalization, which will be the major discussion topic of Section III.

III. EXIT PROPERTIES OF ML-BICM

The mutual information (MI) I between the coded bits $\mathcal{C}\in\{\pm 1\}$ and the LLR ξ is, if the occurrences of $\mathcal{C}=-1$ and $+1$ are equi-probable, given by [16]

$$I=\frac{1}{2}\sum_{\mathcal{C}\in\pm 1}\int_{-\infty}^{\infty} p_{\lambda|c}(\xi|\mathcal{C})\cdot\log_2\left(\frac{2p_{\lambda|c}(\xi|\mathcal{C})}{p_{\lambda|c}(\xi|-1)+p_{\lambda|c}(\xi|+1)}\right)d\xi$$
$$=1-\int_{-\infty}^{\infty} p_{\lambda|c}(\xi|+1)\log_2(1+e^{-\xi})d\xi \tag{17}$$

where $p_{\lambda|c}(\xi|\mathcal{C})=\mathrm{Prob}[\lambda=\xi|c=\mathcal{C}]$ is the pdf of LLR being ξ conditioned upon the coded bit $\mathcal{C}$. Thus, the MI for equalizer and decoder outputs, $I^E_{m,q}$ and $I^D_{m,q}$, respectively, can be calculated by evaluating (17), for which, however, the pdf $p_{\lambda|c}(\xi|\mathcal{C})=\mathrm{Prob}[\lambda=\xi|c=\mathcal{C}]$ has to be

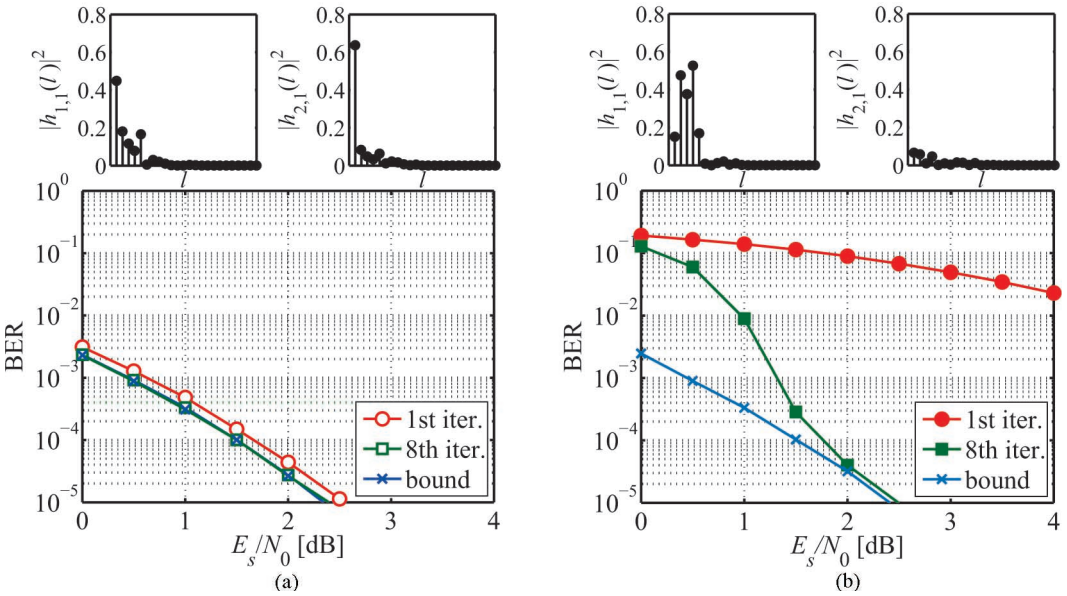

Fig. 2. *BER performances of FD SC-MMSE for QPSK [$Q=2$ in (13)] after the first and eighth iterations, where $M=1$, $N=2$, two 24-path frequency-selective channel realizations, $2K=4096$, $P=64$, and a constraint length 4 nonsystematic half-rate convolutional code are assumed. (a) BER in a good channel realization; (b) in a bad channel realization.*

obtained. An easy way to obtain the pdf is by measuring the histogram of the LLRs $\lambda^a[c_{m,q}(k')]$ and $\lambda^e[c_{m,q}(k')]$ through simulations.

The decoder MI transfer function is denoted by

$$I^D_{m,q} = G_R\left(I^E_{m,q}\right). \tag{18}$$

BER as well as its corresponding frame error rate (FER) can be estimated based on the MI calculated from the decoder's *a posteriori* LLR distribution [16] (referred to as *a posteriori* MI). Fig. 3 shows the relationship between the *a posteriori* MI and BER: The curves on the left-hand side show the equalizer's extrinsic MI I^E (= decoder's *a priori* MI) on the y-axis versus *a posteriori* MI I^P (*Logarithm* of $1-I^P$ is plotted for the notational convenience), and the curves on the right-hand side show I^E versus decoded BER obtained through simulations, for the both of which the constraint length 4 convolutional codes with the rates from 1/8 to 7/8, shown in [27], were used. The vertical lines shown in the figure on the left-hand side correspond to several values of theoretical BER derived from I^P [16]. It is found that the decoder's input I^E values required to achieve theoretical BERs exactly match those values obtained by the simulations.

The simplest case of ML-BICM is with $Q = 2$, with which the equalizer has feedback from only one decoder. Fig. 4 compares the EXIT functions of FD SC-MMSE in two different channels, investigated in Fig. 2, for instantaneous $E_s/N_0 = 0$ dB. It is clearly found that the shape of the equalizer EXIT function depends on the channel realization, and if the equalizer and decoder EXIT functions intersect at a point yielding relatively low decoder output *a posteriori* MI, which is the case of Fig. 2(b), the MI exchange is stuck at the point, and, as shown in Fig. 2(b), high BER results. Conversely, in the channel where the EXIT function's intersection points

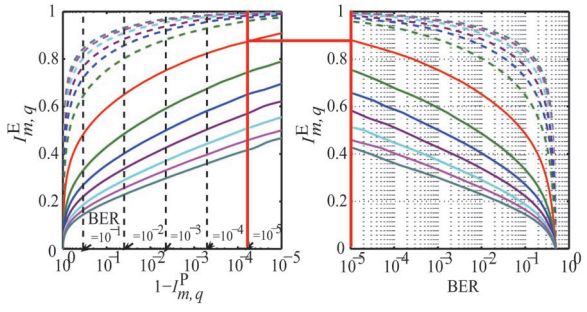

Fig. 3. ***A posteriori* EXIT functions of several constraint length 4 convolutional codes and their corresponding BER curves: The codes shown in Proakis book [27] were used. The rate 2/3–7/8 codes were the punctured codes from the rate 1/2 code.**

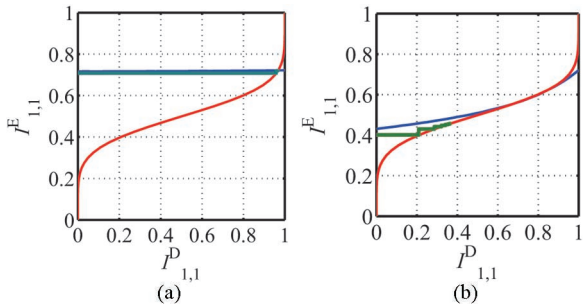

Fig. 4. ***EXIT functions of FD SC-MMSE for instantaneous $E_s/N_0 = 0$ dB in two different channel realizations used in Fig. 2: (a) EXIT in a good channel realization; (b) in a bad channel realization. Dashed lines indicate the MI exchange trajectories.***

yield relatively high decoder output *a posteriori* MI, which is the case in Fig. 2(a), low BER can be achieved.

Despite the ease in calculating the MI of the equalizer output, analyzing for ML-BICM with $Q > 2$ the EXIT characteristic of each layer is not easy, because a certain layer's MI transfer function depends on the other layers', which is formulated as

$$I^E_{m,q} = F_{m,q}\left(I^D_{1,1}, \cdots, I^D_{m,Q/2}, \cdots, I^D_{M,1}, \cdots, I^D_{M,Q/2}\right). \tag{19}$$

This fact makes it difficult to visualize the MI transfer characteristics, even though it is crucial in designing ML-BICM AC techniques to understand how a certain layer has helped the other layers' convergence. An example of the three-dimensional EXIT chart for an ML-BICM equalizer is depicted in Fig. 5 for $M = 1$, $N = 2$, $Q = 4$ (16 QAM), 24-path frequency-selective fading with 2-dB exponential decay factor, and 8-dB symbol energy-to-noise density ratio E_s/N_0. In this case, the EXIT characteristic is expressed by *planes* since each MI depends on the feedback MI from the both decoders of the two layers as

$$I^E_{1,q} = F_{1,q}\left(I^D_{1,1}, I^D_{1,2}\right), \qquad \text{with} \quad (q = 1). \tag{20}$$

It is now found from Fig. 5 that the EXIT *planes* corresponding to the layers $\chi[1,1]$ and $\chi[1,2]$ are separated from each other, because with ML-BICM the constellation is determined, according to (12)–(14), by the super-positioning of multiple small modulation components corresponding to the each layer having different reliabilities. This very important observation boils down to the concept that different code parameters be independently used layer-by-layer so that, as a whole, the total throughput supported by the layers can be

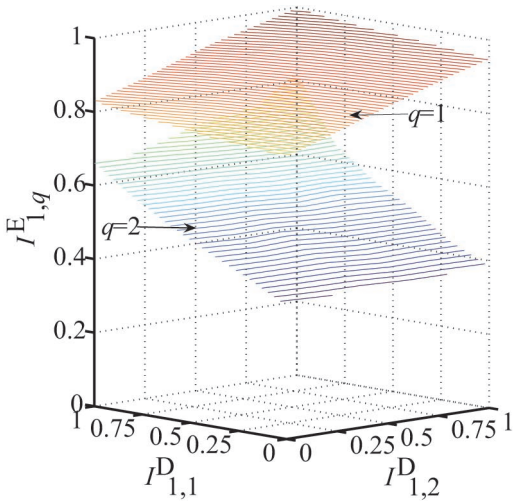

Fig. 5. *Example of the three-dimensional EXIT chart for an ML-BICM equalizer for M = 1, N = 2, Q = 4 (16 QAM), 24-path frequency-selective fading with 2-dB exponential decay factor, E_s/N_0 = 8 dB, 2K = 4096, and ten frames were transmitted for the LLR histogram measurement when drawing the two-dimensional EXIT chart, in order to ensure the accuracy of the pdf evaluation for the MI calculation.*

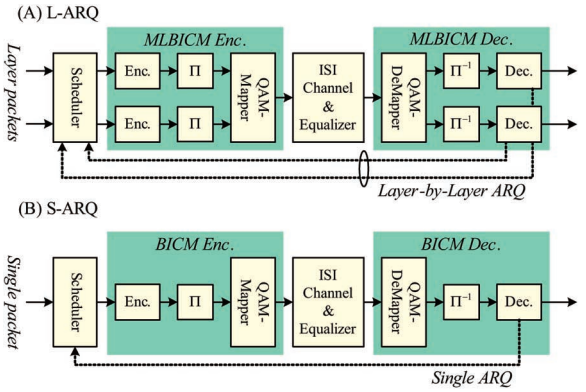

Fig. 6. *Structure of retransmission control with (a) L-ARQ and (b) S-ARQ.*

maximized. The code optimality depends on the channel realization since the *planes* are a time-varying function, and therefore, the selected code information has to be fed back to the transmitter frame by frame.

IV. ADAPTIVE CODING

A. L-ARQ

Now, it should be emphasized that, in ML-BICM, equalization is performed at the symbol level, transmited antenna-by-transmit antenna, and SISO decoding layer-by-layer. Then, to convert the equalizer output symbol to the bit-wise LLR, the MAP algorithm is utilized. Recall that the layers are defined by the "amplitude" of the constellation points; the most crucial point with this structure is that the variance of the bit-wise LLR obtained as the results of the MAP algorithm depends *largely* on its corresponding layer. On the contrary, *standard* BICM has only one encoder-SISO decoder pair, and the transmission does not have a layered structure associated with the constellation points.

The layer separability supported by the ML-BICM invokes an idea that a different code rate is allocated to the each layer, and retransmission controlled independently layer-by-layer. This is reasonable because the different layers achieve different FER, if the frame is constructed for each of the layers independently. This retransmission scheme is referred to as L-ARQ with ML-BICM. Another ARQ scheme, referred to as S-ARQ with BICM, is considered in this paper as a counterpart to L-ARQ, where bits in each frame are S/P-converted, and allocated to the BICM symbols. Fig. 6(a) and (b) represents the logical structures of the retransmission control with L-ARQ and S-ARQ, respectively.

Fig. 7 shows the throughput efficiencies (TPeffs) with the two ARQ schemes, L-ARQ with ML-BICM and S-ARQ with BICM, obtained through simulations, of which parameters are summarized in the figure caption. Assuming infinite buffer selective repeat ARQ, TPeff for S-ARQ was calculated from FER by

$$\text{TPeff} = R(1 - \text{FER}) \tag{21}$$

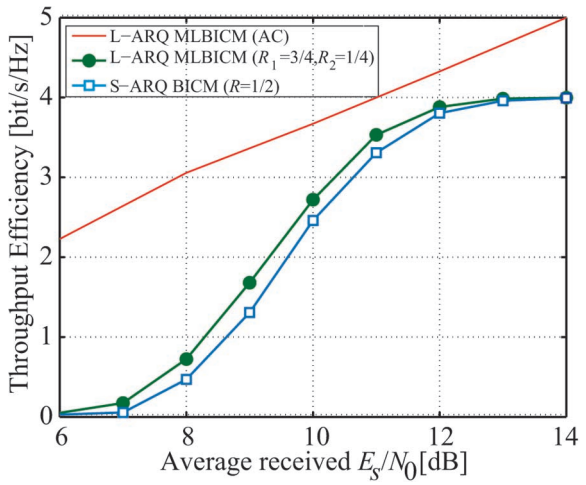

Fig. 7. *Throughput efficiencies (TPefffs) with the three ARQ schemes, S-ARQ with BICM, L-ARQ with ML-BICM, and L-ARQ with ML-BICM AC: M = 1, N = 2, two 24-path frequency-selective channel realizations, 2K = 4096, and P = 64 are assumed. A constraint length 4 nonsystematic half-rate convolutional code is assumed for S-ARQ with BICM. A rate 1/4 code and a rate 3/4 codes, both with constraint length 4, are assumed for Layers 1 and 2, respectively, of L-ARQ with ML-BICM.*

where R is the rate of the code used for the turbo equalization. For L-ARQ, TPeff is defined by the ratio of the total number of the information bits received without error-to-the-number of the total transmitted bits. Simulation parameters are summarized in the caption of Fig. 7, where for fair comparison the total bit number to be transmitted per second is kept constant for the all schemes. For L-ARQ, the maximum TPeff of each layer is scaled to match the spectral efficiency of the layer. It is found that L-ARQ can achieve better TPeff in low SNR range than S-ARQ. This is because of the layer-separability advantage with the ML-BICM L-ARQ: With S-ARQ, the retransmission probability is dominated by errors from the signal point having lower SNR in the constellation. It should be recognized that this comparison is not completely fair due to the larger frame length of BICM, which slightly inflates the mean FER. Shortening the frame length with BICM is problematic, however, due to convergence problems with short interleaving.

B. L-ARQ With EXIT-Based Adaptive Code Selection

Despite the throughput merit achieved by ML-BICM with L-ARQ, there still remains a mismatch between the given channel realization and coding scheme used by the each layer, because the same code is used by the layers for ML-BICM turbo equalization, regardless of the channel conditions. The mismatch may lead the system to two detrimental situations: 1) The code redundancy is too high to maintain the information rate inherently bearable by the channel itself; 2) the turbo equalization does not converge. This implicitly means that if the code parameters are adaptively selected at each of the ML-BICM layers for turbo equalization, further throughput improvement can be provisioned. This section introduces a code selection technique to reduce the code-equalizer mismatch.

Several techniques are known that aim to achieve the best matching between equalizer and channel code used [17]–[19]. Basically, the turbo equalization system is a serially concatenated system, and therefore, the code-equalizer optimal matching can be achieved by the EXIT curve fitting technique, which is well known for the optimal design of low-density parity check (LDPC) codes. References [17]–[19] use a curve-fitting technique for the serially concatenated binary convolutional coded turbo equalization. In fact, the curve-fitting technique for code optimization can be extended to a nonbinary case with the aim of deriving trellis turbo codes for BICM, where symbol-wise MI has to be used instead of binary MI. However, it is still unknown how UEP can best be exploited with the symbol-based code design.

The major difficulty of ML-BICM AC lies in the fact that convergence property of the each layer is NOT independent, as shown in Section IV-A the previous subsection when describing the multidimensional EXIT chart. Therefore, it may be possible to optimize the codes based on the area property analysis. In practice, however, it is not feasible to perform the multidimensional EXIT analysis on-line, given the channel realizations with the MIMO setup, because of the computational complexity. Therefore, it is more practical to *select* the codes from among the predetermined code set rather than to *optimize* the code on-line.

Reference [20] proposes for *layer-by-layer* ML-BICM adaptive transmission a practical technique for the code *selection* based on the *partial* EXIT analysis at the receiver side, which does not fully analyze the EXIT plane, but only limited points in the trajectory are evaluated using the received signal by an empirical formula [21] for the MI calculation. The transmitter is then notified of the selected codes for the each layer via the feedback channel, and uses the selected codes for the next transmission, assuming that the CSI stays the same at least over two consecutive frames. Reference [21]'s selection technique is further extended to achieve better performance [22], which is summarized below.

1) For the each Tx antenna's each layer, evaluate the equalizer output MI corresponding to the following two points:
   a) after the first iteration, and
   b) after the last iteration, where the decoder does not increase its output MI.

   The equalizer output MI corresponding to the points a) and b) are denoted as $I_{m,q}^{E(\mathrm{Start})}$ and $I_{m,q}^{E(\mathrm{End})}$, respectively. $I_{m,q}^{E(\mathrm{Start})}$ can be calculated directly from the equalizer output, and $I_{m,q}^{E(\mathrm{End})}$ by substituting the decoder output MI into the inverse EXIT function of each decoder, both using [21].
2) To minimize the rate loss, select a set R_{c1} of codes of which rates R satisfy

$$R_{c1} \in \left\{ R | \gamma_R^{\alpha} < I_{m,q}^{E(\mathrm{End})} \right\} \tag{22}$$

   in the code set, where γ_R^{α} denotes the equalizer output MI required to yield FER $\leq \alpha$.
3) To avoid the intersection between the two curves before decoder output MI reaches a value close to 1.0, select a set R_{c2} of codes of which rates R satisfy

$$R_{c_2} \in \left\{ R | \gamma_R^{\beta} < I_{m,q}^{E(\mathrm{Start})} \right\} \tag{23}$$

   in the code set, where γ_R^{β} denotes the equalizer output MI required yielding decoder output MI at the first iteration larger than the value β. The

condition (3) is equivalent to $I_{m,q}^{D(\mathrm{Start})} > \beta$, where $I_{m,q}^{D(\mathrm{Start})}$ is the decoder output MI at the first iteration.

4) Allocated the code rate $R_{m,q}$ satisfying

$$R_{m,q} \in \max\{R_{c1} \cap R_{c2}\}. \tag{24}$$

5) If $R_{c1} \cap R_{c2} = \phi$, $R_{m,q} =$ [the lowest rate in the available code set].

6) The selected code is used in the next frame transmission. This algorithm has two design parameters, α and β, of which corresponding MI γ_R^{α} and γ_R^{β}, respectively, have to be precalculated for each code in the code set.

C. Throughput of L-ARQ With ML-BICM AC

Results of simulations presented in [22] are summarized in this subsection to demonstrate the throughput enhancement achieved by the L-ARQ with ML-BICM AC over fixed rate L-ARQ, described in Section III. Sixteen QAM and a spatially uncorrelated 2×2 MIMO system were assumed. The other simulation parameters are the same as that used for the throughput simulations for S-ARQ with BICM and L-ARQ with ML-BICM. Perfect knowledge about the channels was assumed available at the receiver. The max-log-MAP algorithm with a correcting factor proposed by [23] was used in the each layer's SISO decoder, and the receiver performed eight iterations of the equalization and decoding chain. The design parameters α and β are set at 0.1 and 0.15, respectively.

Ideal selective repeat ARQ was assumed, as in Section III. The average throughput is defined by the ratio of the total number of the information bits received without error-to-the-number of the total transmitted bits, where fading variations on the path components were assumed to be complex-Gaussian distributed, and kept constant during each S-ARQ period while statistically independent fading realizations were assumed in different ARQ periods. Fig. 7 shows, together with S- and L-ARQ without AC, average TPeff of L-ARQ with ML-BICM AC versus average received E_s/N_0. Fig. 8 indicates the *cumulative* throughput efficiencies that sum up the transmitted bits, received correctly, in the increasing order of the layers, where simulation parameters are the same as that for Fig. 7. It is found by making a comparison between Figs. 7 and 8 that ML-BICM AC can significantly improve the throughput performance over the fixed code rate ARQ: Because the code rate is fixed for any channel realizations without AC, the layers $\chi[1,2]$ and $\chi[2,2]$ do not make any significant contributions to the total throughput when average $E_s/N_0 < 10$ dB; in contrast, L-ARQ with ML-BICM AC allows the layers to adaptively adjust the code rates, given channel realizations, by which all layers make contributions to the total throughput.

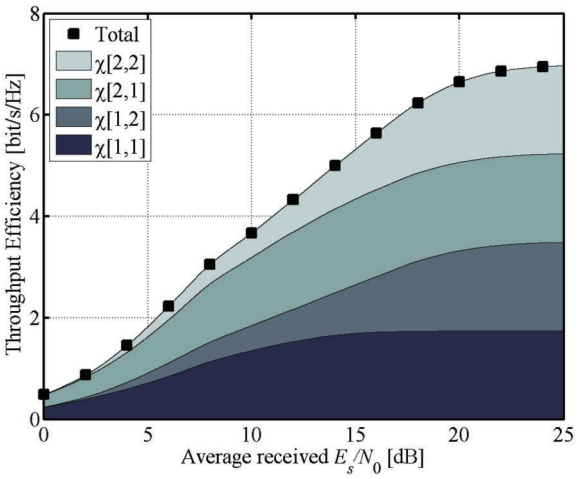

Fig. 8. *Cumulative throughput efficiencies of L-ARQ with ML-BICM AC that sum up the transmitted bits, received correctly, in the increasing order of the layers; $M = 2$, $N = 2$, $Q = 4$ (16 QAM), 24-path frequency-selective channel realizations, $2K = 4096$, and $P = 64$ are assumed.*

V. OUTAGE-BASED AC

In the previous sections, we assumed that the instantaneous CSI representing the channel matrix $\boldsymbol{H}$ is available at the receiver, and that the code selection and feedback are based on the instantaneous CSI. However, in practice, it is difficult to know the exact values of the elements of the channel matrix $\boldsymbol{H}$. The inaccuracy of the knowledge of $\boldsymbol{H}$ is due to the following.

1) The channel matrix has to be estimated by using the training sequences, which is located in each frame to be equalized, and of which timing and waveform are known to the receiver. The accuracy of the channel estimation is determined by the received SNR, the length of the training sequence, and the number of the channel parameters that have to be estimated. The training length is limited to a certain number yielding the acceptable overhead ratio.

2) The EXIT-based code selection technique is based on the assumption that the CSI stays the same at least over two consecutive frames. However, in the presence of the user mobility, the channel matrix estimated by receiving the first frame may be outdated when the second frame is received. This leads to *another* mismatch between the selected code and the equalization convergence property for the channel, when the second frame is transmitted.

Therefore, in those cases, instead of pursuing the code-equalizer optimization for the adaptive transmission based on the instantaneous CSI measurement, seeking for outage-based optimization should be more practical. In the presence of channel estimation error, the equalizer output extrinsic MI becomes a random variable, and the EXIT curves distribute even though they are from the same

actual channel realization. Then, an idea arises that a line representing a certain percentage, say, P%, of the cumulative probability of EXIT curves is first drawn, and the code parameters are determined so that the optimal matching between the equalizer's P% EXIT and the code EXIT curves is then sought for. With the codes satisfying this optimality definition, FER $= P$% can be achieved even in the presence of the channel estimation error. Furthermore, if only the average CSI is available at the receiver, P% outage-based code optimization is still possible, where the EXIT curve distribution is due to the variation of the channel realizations that are the samples from the same average CSI. Reference [17] utilizes the outage-based code optimization technique for the optimal matching between LDPC code and FD SC-MMSE turbo equalizer, where only average CSI is assumed available at the receiver.

VI. MEASUREMENT DATA-BASED PERFORMANCE VERIFICATION

Recent advances in channel sounding techniques [24], [25] make it possible to analyze the channels in realistic conditions. The sequence of impulse response of the channel between any of the Tx and Rx antenna pairs in the MIMO system can be recorded in real time. This technique is sometimes referred to as "multidimensional channel sounding." By analyzing the recorded data, we can identify how propagation medium has behaved in the spatial and temporal domains, represented by direction-of-departure and direction-of-arrival, both in azimuth and elevation domains, and time-of-arrival of the component signals.

Another beneficial point with real-time multidimensional channel sounding is that the recorded CIR data can be used for realistic off-line simulations for signal transmission techniques. Since the data represents the real propagation scenario, in-field performances can be accurately evaluated by running simulations for signal processing algorithms of interest using the measurement data. This technique provides us with far more realistic performance estimates than model-based simulations. Furthermore, the performance curves can be correlated with the multidimensional channel analysis results, by which the performance tendency can be well understood in reflection to the physical propagation phenomena.

It is now interesting to know how the ARQ schemes investigated in this paper behave in realistic conditions, covering non-line-of-sight (NLOS) and LOS propagation conditions, and how the code parameters are adjusted to enhance the total throughput in those conditions. Results of simulations for S-ARQ with BICM, L-ARQ with ML-BICM, and L-ARQ with ML-BICM AC are presented in this section.

A large set of CIR data[2] collected by using a bidirectional multidimensional channel sounding measurement campaign that took place in a large courtyard at the campus of Ilmenau University of Technology, Germany, is used.

A map of the measurement site is shown in Fig. 9(a). A 16-element uniform circular array (UCA) with minimum element spacing of half the wave length and eight-element uniform linear array (ULA) with element spacing of 0.4 wavelength were used as the Tx and Rx antennas, respectively. The transmitter was moved at a walking speed along the route marked by the dashed line in the figure, and the receiver position was fixed. The area was surrounded by buildings of which height was approximately 15 m, and there was a metal object on the front-side angle of the receiver array. The first 3 m of the measurement route is behind the metal object, and therefore, this section is characterized as an NLOS part. The major specifications of the measurement campaign are summarized in the footnote of Fig. 9.

Fig. 9(b) shows root-mean-squared (rms) azimuth spreads at both the Tx and Rx sides, obtained by using

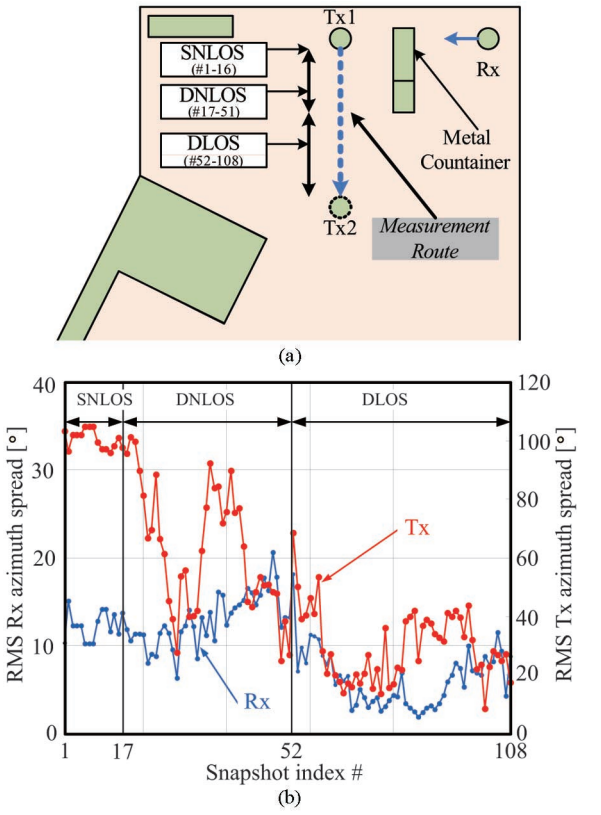

Fig. 9. *(a) Map of the measurement route; (b) rms azimuth spreads at the Tx and Rx sides: 5.2-GHz sounding carrier frequency, 120-MHz measurement bandwidth, 16-element UCA with minimum element spacing of 0.5 wave length for Tx located at approximately 2.1 m high, eight-element ULA with minimum element spacing of 0.4 wave length for Rx located at approximately 1.6 m high, 20 Msymbols/s, and 0.25 roll-off factor are assumed.*

[2][Online]. Available: http://www.channelsounder.de/csdexample.htm.

the gradient search-based maximum likelihood estimation framework [26], versus the snapshot number. The total number of snapshots gathered along the measurement route is 108. It is found that snapshot #52 is a border point between NLOS and LOS. Snapshots #1 and #16 were referred to as static NLOS (SNLOS) because Tx was fixed behind the metal object. Snapshots #17–#51 and #52–#108 are refereed to as dynamic NLOS (DNLOS) and dynamic LOS (DLOS), respectively. Two antenna elements having the largest spacing, located on the diameter of the UCA, and on the both ends of the ULA, at Tx and Rx, respectively, were used, resulting in 2×2 MIMO channels. The spacing of the two antenna elements used was 2.56 and 2.8 times the wavelength, respectively, at Tx and Rx.

Fig. 10(a), (b), and (c) show TPeffs with S-ARQ with BICM, L-ARQ with ML-BICM, and L-ARQ with ML-BICM AC, respectively, versus snapshot number,[3] where the curves indicate cumulative TPeff supported by the layers. The simulation parameters are the same as those used in the model-based simulations presented in Section V. The received *instantaneous* E_s/N_0 value was kept at 15 dB. The figure clearly shows the variation in azimuth spread is a dominating factor for the throughput efficiency when received instantaneous E_s/N_0 is fixed. It is found that in the LOS environments, the throughput can only reach approximately 80 Mb/s, although 105 Mb/s is achieved in NLOS environment. This is because the less scattering-rich, the lower the azimuth spreads in LOS environments, as shown in Fig. 9, resulting in the lower channel capacity of the MIMO systems.

VII. CONCLUSIONS AND FUTURE WORK

In this paper, we have introduced an AC technique for multilevel BICM broadband single-carrier signaling assuming turbo equalization. An effective use of the separability among the ML-BICM layers supported by the maximum MAP algorithm makes it possible optimize layer-wise error control independently of other layers, for which turbo equalization uses the decoder feedback from the each layer. In contrast to this structure, conventional BICM turbo equalization has one turbo loop connecting the detector and decoder, separated by interleaver and deinterleaver, resulting in the fact that the decoder's input bit-wise LLR depends on SNR of the constellation point which each bit has been mapped to.

One approach to utilizing the layer separability well is automatic repeat request by each layer that uses a different

[3]TPeff is evaluated snapshot by snapshot, which presumably indicates that the retransmissions complete only at one single snapshot. It is out of the scope of this paper to consider that retransmissions take place using different snapshots, and therefore, neither instantaneous fading nor shadowing variations are taken into account.

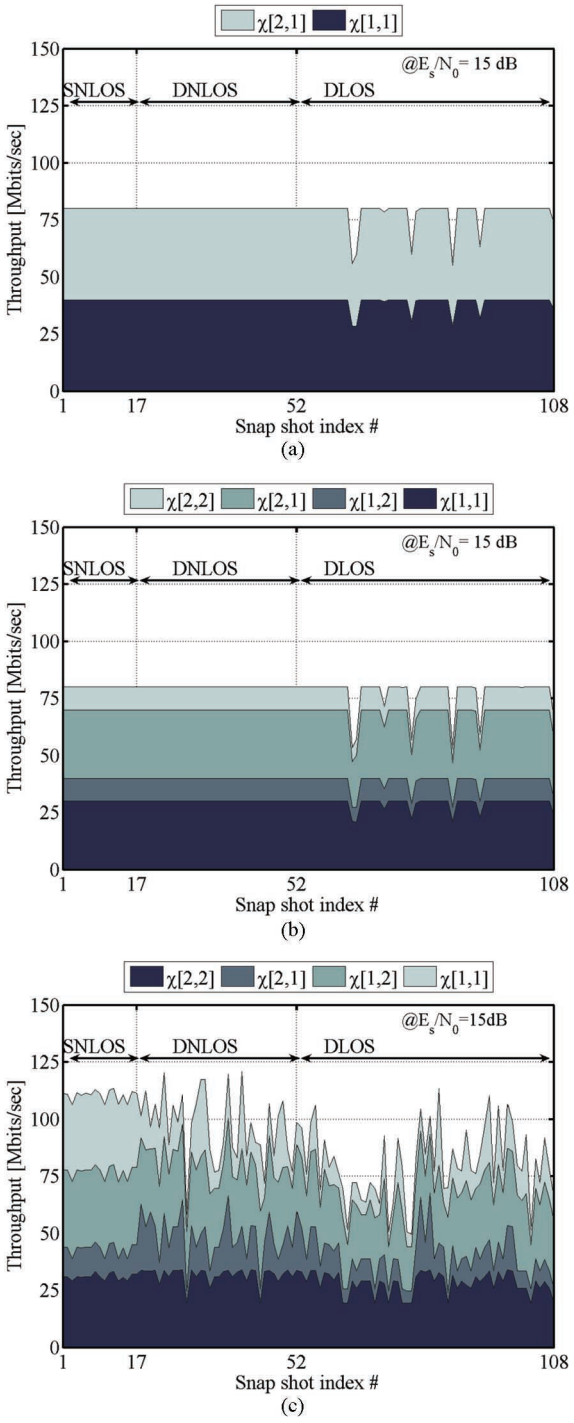

Fig. 10. *TPeffs versus snapshot number, where the curves indicate cumulative TPeff supported by the layers: (a) S-ARQ with BICM; (b) L-ARQ with ML-BICM; (c) L-ARQ with ML-BICM AC. A constraint length 4 nonsystematic half-rate convolutional code is assumed for S-ARQ with BICM. A rate 1/4 code and a rate 3/4 codes, both with constraint length 3, are assumed for Layers 1 and 2, respectively, of L-ARQ with ML-BICM.*

code, referred to as L-ARQ in this paper. It has been shown that L-ARQ can achieve higher total throughput than retransmission with BICM turbo equalization governed by an S-ARQ. This is because with L-ARQ, retransmission takes place only within the same layers, and the frames are constructed with the bits having the same LLR variance, while with S-ARQ, the frames are constructed from the different layers.

One drawback with L-ARQ is that it does not change the code parameters for turbo equalization, regardless of the channel realization; if the code parameters such as the rate and the generator polynomials can be determined so that the selected code is well matched to the equalizer's convergence properties with each layer, the total throughput can further be improved over the L-ARQ scheme. This technique is referred to as L-ARQ with ML-BICM AC. To avoid the necessity for performing multi-dimensional EXIT analysis for ML-BICM AC, an empirical technique for the code selection has been introduced. It has been shown that L-ARQ with ML-BICM AC can achieve much higher total throughput than S-ARQ with fixed code.

However, it is obvious that with L-ARQ with ML-BICM AC, the total throughput still plateaus at the sum of the code rates allocated for the both schemes, even when the received E_s/N_0 becomes large enough. Obviously, this problem can be solved by jointly exploiting the degrees-of-freedom supported by the code selection and the modulation multiplicity. Pursuing the real optimality of modulation and coding with ML-BICM for broadband single-carrier signaling is still at its basic research stage. ■

REFERENCES

[1] B. Vucetic and J. Yuan, *Turbo Codes: Principles and Applications*. Norwell, MA: Kluwer, 2000.

[2] D. Reynolds and X. Wang, "Low complexity turbo-equalization for diversity channels," *IEEE Trans. Signal Process.*, vol. 81, no. 5, pp. 989–995, May 2001.

[3] M. Tüchler and J. Hagenauer, "Turbo equalization using frequency domain equalizers," in *Proc. Allerton Conf.*, Monticello, IL, Oct. 2000, pp. 1234–1243.

[4] M. Tüchler, A. C. Singer, and R. Koetter, "Minimum mean squared error equalization using *a priori* information," *IEEE Trans. Signal Process.*, vol. 50, no. 3, pp. 673–683, Mar. 2002.

[5] T. Abe and T. Matsumoto, "Space-time turbo equalization in frequency-selective MIMO channels," *IEEE Trans. Veh. Technol.*, vol. 52, no. 3, pp. 469–475, May 2003.

[6] D. Falconer, S. L. Ariyavisitakul, A. Benyamin-Seeyar, and B. Eidson, "Frequency domain equalization for single-carrier broadband wireless systems," *IEEE Commun. Mag.*, vol. 40, no. 4, pp. 58–66, Apr. 2002.

[7] H. Sari, G. Karam, and I. Jeanclaud, "Frequency domain equalization of mobile radio and terrestrial broadcast channels," in *Proc. IEEE Globcom*, San Francisco, CA, Nov. 1994, pp. 1–5.

[8] N. Al-Dhahir, "Single-carrier frequency-domain equalization for space-time-coded transmissions over broadband wireless channels," in *Proc. IEEE Int. Symp. Personal, Indoor, and Mobile Radio Communications (PIMRC)*, San Diego, CA, Sep. 2001, pp. 143–146.

[9] M. Yee, M. Sandell, and Y. Sun, "Comparison study of single-carrier and multi-carrier modulation using iterative based receiver for MIMO systems," in *Proc. IEEE Vehicular Technology Conf.*, Milan, Italy, May 2004, pp. 1275–1279.

[10] K. Kansanen and T. Matsumoto, "An analytical method for MMSE MIMO turbo equalizer EXIT chart computation," *IEEE Trans. Wireless Commun.*, vol. 6, no. 1, pp. 59–63, Jan. 2007.

[11] B. Ng, D. Falconer, K. Kansanen, and N. Veselinovic, "Frequency-domain methods for detection and estimation," in *Proc. 14th Int. IST Mobile and Wireless Summit*, Dresden, Germany, 2005.

[12] A. Dejonghe and L. Vandendorpe, "Bit-interleaved turbo equalization over static frequency selective channels: Constellation mapping impact," *IEEE Trans. Commun.*, vol. 52, no. 12, pp. 2061–2065, Dec. 2004.

[13] K. Kansanen and T. Matsumoto, "Turbo equalization of multilevel coded QAM," in *Proc. IEEE Workshop Signal Processing Advances in Wireless Communications*, Rome, Italy, 2003.

[14] K. Kansanen, C. Schneider, T. Matsumoto, and R. Thomä, "Multilevel coded QAM with MIMO turbo-equalization in broadband single-carrier signaling," *IEEE Trans. Veh. Technol.*, vol. 54, no. 3, pp. 954–966, May 2005.

[15] L. Hanzo, T. H. Liew, and B. L. Yeap, *Turbo Coding, Turbo Equalization and Space-Time Coding for Transmission Over Fading Channels*. New York: Wiley, 2002.

[16] S. ten Brink, "Convergence behavior of iteratively decoded parallel concatenated codes," *IEEE Trans. Commun.*, vol. 49, no. 10, pp. 1727–1737, Oct. 2001.

[17] R. Wohlgenmant, K. Kansanen, D. Tujkovic, and T. Matsumoto, "Outage-based LDPC code design for SC/MMSE turbo equalization," in *Proc. IEEE Vehicular Technology Conf.*, Stockholm, Sweden, May 2005, pp. 505–509.

[18] J. Wang, S. X. Ng, A. Wolfgang, L. L. Yang, S. Chen, and L. Hanzo, "Near-capacity three-stage MMSE turbo equalization using irregular convolutional codes," in *Proc. ITG Turbo Coding Conf.*, Munich, Germany, 2006.

[19] J. Wang, S. X. Ng, L. L. Yang, and L. Hanzo, "Combined serially concatenated codes and MMSE equalization: An EXIT chart perspective," in *Proc. IEEE Vehicular Technology Conf.*, Montreal, Canada, Sep. 2006, pp. 1–5.

[20] S. Ibi, T. Matsumoto, S. Sampei, and N. Morinaga, "EXIT chart-aided adaptive coding for MMSE turbo equalization with multilevel BICM signaling," *IEEE Commun. Lett.*, vol. 10, no. 6, pp. 486–488, Jun. 2006.

[21] J. Hagenauer, "The EXIT Chart-Introduction to extrinsic information transfer in iterative processing," in *Proc. Eur. Signal Processing Conf. (EUSIPCO)*, 2004, pp. 1541–1548.

[22] S. Ibi, T. Matsumoto, R. Thomä, S. Sampei, and N. Morinaga, "EXIT chart-aided adaptive coding for multilevel BICM turbo equalization in frequency selective MIMO channels," *IEEE Trans. Veh. Technol.*, to be published.

[23] P. Robertson, E. Villebrun, and P. Hoeher, "A comparison of optimal and sub-optimal MAP decoding algorithms operating in the log domain," in *Proc. ICC*, Seattle, WA, 1995, pp. 1009–1013.

[24] R. Thomä, M. Landmann, A. Richter, and U. Trautwein, "Multi-dimensional high-resolution channel sounding," in *Smart Antennas in Europe—State-of-the-Art, EURASIP, Book Series*. EURASIP Book Series on SP&C, New York: Hindawi Publishing Corporation, 2005.

[25] R. Thomä, D. Hampicke, A. Richter, G. Sommerkorn, C. Schneider, U. Trautwein, and W. Wirntzer, "Identification of time-varying directional mobile radio channels," *IEEE Trans. Instrum. Meas.*, vol. 49, no. 2, pp. 357–364, Apr. 2000.

[26] R. Thomä, M. Landmann, and A. Richter, "RIMAX—A maximum likelihood framework for parameter estimation in multidimensional channel sounding," in *Proc. Int. Symp. Antenna and Propagation*, Sendai, Japan, Aug. 2004.

[27] J. G. Proakis, *Digital Commun.* New York: McGraw-Hill, 2001.

ABOUT THE AUTHORS

Tad Matsumoto (Senior Member, IEEE) received the B.S., M.S., and Ph.D. degrees from Keio University, Yokohama, Japan, in 1978, 1980, and 1991, respectively, all in electrical engineering.

He joined Nippon Telegraph and Telephone Corporation (NTT) in April 1980, where he was involved in a lot of research and development projects, all for mobile wireless communications systems. In July 1992, he transferred to NTT DoCoMo, where he researched code-division multiple-access techniques for mobile communication systems. In April 1994, he transferred to NTT America, where he served as a Senior Technical Advisor of a joint project between NTT and NEXTEL Communications. In March 1996, he returned to NTT DoCoMo, where he was the Head of the Radio Signal Processing Laboratory until August of 2001, when he worked on adaptive signal processing, multiple-input–multiple-output turbo signal detection, interference cancellation, and space–time coding techniques for broadband mobile communications. From 1992 to 1994, he served as a part-time Lecturer at Keio University. In May 2002, he moved to Oulu University, Oulu, Finland, where he is currently a Professor with the Centre for Wireless Communications. He served as a Visiting Professor at Ilmenau University of Technology, Ilmenau, Germany, funded by the German MERCATOR Visiting Professorship Program, until January 2007. Since April 2007, he has been serving as a Professor at Japan Advanced Institute of Science and Technology (JAIST), Japan, while also keeping the current position at the University of Oulu.

Dr. Matsumoto is a recipient of IEEE VTS Outstanding Service Award (2001), Nokia Foundation Visiting Fellow Scholarship Award (2002), IEEE Japan Council Award for Distinguished Service to the Society (2006), IEEE Vehicular Technology Society James R. Evans Avant Garde Award (2006), and Thuringen State Research Award for Advanced Applied Science (2006). He served as a member of the Board-of-Governors of the IEEE Vehicular Technology Society from January 2002 to December 2004 and is now serving from January 2005 to December 2007. Recently, he has been re-elected as a board member of the society from January 2008 to December 2010. He has been appointed a Finnish Distinguished Professor from January 2008 to December 2012, funded by the Finnish National Technology Agency (Tekes) and Finnish Academy.

Shinsuke Ibi (Member, IEEE) was born in Nagoya, Japan, in 1978. He received the B.E. degree in advanced engineering from Suzuka College of Technology, Japan, in 2002, and the M.E. and Ph.D. degrees from Osaka University, Osaka, Japan, in 2004 and 2006, respectively.

During 2005 to 2006, he was at Centre for Wireless Communications, University of Oulu, Finland, as a Visiting Researcher. In 2007, he joined the Faculty of Engineering, Osaka University, and is currently an Assistant Professor in the Department of Information and Communications Technology, Osaka University. His research interests include EXIT-based coding theory, iterative decoding, multiuser detection, and communication theory.

Dr. Ibi received the third YRP Encouragement Award, the IEEE VTS Japan 2003 Young Researcher's Encouragement Award, and the IEICE 2004 Active Research Award in Radio Communication Systems.

Seiichi Sampei (Fellow, IEEE) was born in Yokohama, Japan, in 1957. He received the B.E., M.E., and Ph.D. degrees in electrical engineering from Tokyo Institute of Technology, Tokyo, Japan, in 1980, 1982, and 1991, respectively.

From 1982 to 1993, he was engaged in the development of adjacent channel interference rejection, fast fading compensation, and M-ary QAM techniques for land-mobile communication systems, as a Researcher in the Communications Research Laboratory, Ministry of Posts and Telecommunications, Japan. During 1991 to 1992, he was at the University of California, Davis, as a Visiting Researcher. In 1993, he joined the Faculty of Engineering, Osaka University, and he is currently a Professor in the Department of Information and Communications Technology, Osaka University, where he has developed adaptive modulation, intelligent radio transmission/access, and cognitive wireless networking techniques.

Dr. Sampei received the Shinohara Young Engineering Award, the Achievements Award from the Institute of Information and Communication Engineers (IEICE), the Telecom System Technology Award from the Telecommunication Advancement Foundation, and the DoCoMo Mobile Science Award from Mobile Communication Fund. He is a member of the Institute of Image Information and Television Engineers (ITE) and a fellow of the IEICE.

Reiner Thomä (Fellow, IEEE) received the Dipl.-Ing., Dr.-Ing., and Dr.-Ing. habil. degrees in electrical engineering (information technology) from Ilmenau University of Technology, Germany, in 1975, 1983, and 1989, respectively.

Since 1992, he has been a Professor of Electrical Engineering (Electronic Measurement Engineering) at Ilmenau University of Technology. He is involved in various German and European research clusters, European network of excellence NEWCOM, and he is the speaker of the German national research program "Ultrawide-Band Radio Technologies for Communication, Localization and Sensor Technology." His research interests include digital signal analysis, sensor array signal processing, parameter estimation, and system identification methods and their application in mobile radio propagation measurement and UWB sensor systems. This includes multidimensional propagation parameter estimation techniques, source localization, and position tracking.

Dr. Thomä is a member of VDE/ITG and URSI (Comm.A). He is Chairman of the IEEE Instrumentation and Measurement Society Technical Committee TC-13 "Wireless and Telecommunications."